VIRAL IMMUNOLOGY
Volume 31, Number 3, 2018

Pp. 206–222
DOI: 10.1089/vim.2017.0051

Original Articles

Lung Vascular Remodeling, Cardiac Hypertrophy, and Inflammatory Cytokines in SHIV*nef*-Infected Macaques

Sharilyn Almodovar,[1,2] Jessica Swanson,[1] Luis D. Giavedoni,[3] Sreetharan Kanthaswamy,[4] Carlin S. Long,[5] Norbert F. Voelkel,[6] Michael G. Edwards,[1] Joy M. Folkvord,[7] Elizabeth Connick,[7] Susan V. Westmoreland,[8] Paul A. Luciw,[9] and Sonia C. Flores[1]

Abstract

Fatal pulmonary arterial hypertension (PAH) affects HIV-infected individuals at significantly higher frequencies. We previously showed plexiform-like lesions characterized by recanalized lumenal obliteration, intimal disruption, medial hypertrophy, and thrombosis consistent with PAH in rhesus macaques infected with chimeric SHIV*nef* but not with the parental SIVmac239, suggesting that Nef is implicated in the pathophysiology of HIV-PAH. However, the current literature on non-human primates as animal models for SIV(HIV)-associated pulmonary disease reports the ultimate pathogenic pulmonary outcomes of the research efforts; however, the variability and features in the actual disease progression remain poorly described, particularly when using different viral sources for infection. We analyzed lung histopathology, performed immunophenotyping of cells in plexogenic lesions pathognomonic of PAH, and measured cardiac hypertrophy biomarkers and cytokine expression in plasma and lung of juvenile SHIV*nef*-infected macaques. Here, we report significant hematopathologies, changes in cardiac biomarkers consistent with ventricular hypertrophy, significantly increased levels of interleukin-12 and GM-CSF and significantly decreased sCD40 L, CCL-2, and CXCL-1 in plasma of the SHIV*nef* group. Pathway analysis of inflammatory gene expression predicted activation of NF-κB transcription factor RelB and inhibition of bone morphogenetic protein type-2 in the setting of SHIV*nef* infection. Our findings highlight the utility of SHIV*nef*-infected macaques as suitable models of HIV-associated pulmonary vascular remodeling as pathogenetic changes are concordant with features of idiopathic, familial, scleroderma, and HIV-PAH.

Keywords: SHIV*nef*, pathogenesis, pulmonary vascular remodeling, inflammation

Introduction

With the advent of antiretroviral therapy, human immunodeficiency virus (HIV) infection is now a manageable chronic disease. Nonetheless, HIV-infected individuals face long-term complications including pulmonary arterial hypertension (PAH). Life-threatening PAH is relatively rare (10–50 individuals *per* million) but afflicts HIV-infected individuals at significantly higher frequencies (1 in 200) regardless of antiretroviral drug status, HIV viral load, CD4 counts, or duration of HIV infection (42). HIV-associated PAH (HIV-PAH) is clinically indistinguishable from other forms of PAH, and is characterized by high pulmonary artery pressures, inflammation, pulmonary vascular remodeling, increased circulating inflammatory cytokines, and the presence of cells that obliterate the lumina of pulmonary arteries and form plexiform lesions. There is no definitive proof that HIV directly causes PAH or infects pulmonary endothelial cells. Nevertheless, HIV proteins play key roles in PAH-associated pulmonary vascular remodeling

[1]Division of Pulmonary Sciences and Critical Care Medicine, University of Colorado Anschutz Medical Campus, Aurora, Colorado.
[2]Department of Immunology and Molecular Microbiology, Texas Tech University Health Sciences Center, Lubbock, Texas.
[3]Department of Virology and Immunology, and Southwest National Primate Research Center, Texas Biomedical Research Institute, San Antonio, Texas.
[4]School of Mathematical and Natural Sciences, New College of Interdisciplinary Arts and Sciences, Arizona State University, Arizona.
[5]Department of Medicine, University of California, San Francisco, San Francisco, California.
[6]Victoria Johnson Center for Obstructive Lung Diseases, Virginia Commonwealth University, Richmond, Virginia.
[7]Division of Infectious Diseases, Department of Medicine, University of Arizona College of Medicine, Tucson, Arizona.
[8]New England Primate Research Center, Division of Comparative Pathology, Southborough, Massachusetts.
[9]Center for Comparative Medicine, University of California, Davis, Davis, California.

because their interactions with molecular partners in the infected cells induce inflammation, oxidative stress, and deregulate apoptosis and proliferation of vascular endothelial cells (9,12,18,25).

Non-human primates infected with simian immunodeficiency virus (SIV) recapitulate many aspects of HIV pathogenesis and end organ diseases. Chalifoux *et al.* reported intimal and medial thickening in pulmonary arteries, and pulmonary thrombosis with recanalization in rhesus macaques infected with SIVmac251 strain (6). George *et al.* reported similar pulmonary vascular changes in SHIV$env_{89.6P}$-infected cynomolgus macaques and $SIV_{\Delta B670}$-infected rhesus macaques, including occasional plexiform lesions characterized mostly by collagen deposition and significantly elevated right atrial, right ventricular systolic, and pulmonary artery pressures (14,15). Pulmonary vascular remodeling consistent with PAH was also reported in morphine-treated rhesus macaques infected with SIVmacR71/17E (44). In addition, pulmonary arterial occlusive thrombi were reported in two macaques infected with an engineered microglia-tropic SHIV-B0159 N4-p2 at 73 weeks postinfection (WPI) (10). We previously showed plexiform-like lesions characterized by recanalized lumenal obliteration, intimal disruption, medial hypertrophy, and thrombosis consistent with PAH in rhesus macaques infected with chimeric virions expressing human HIVnef in an SIVmac239 genetic backbone (SHIV*nef*), but not in macaques infected with the parental SIVmac239. The SIV-infected animals exhibited lung pathology without pulmonary vascular lesions (33,34). In addition, we reported that HIV Nef protein co-localizes with endothelial cells and mediates Golgi fragmentation in PAH-like plexiform lesions in macaques infected with SHIV*nef*, suggesting a direct pathogenetic relationship (31,33,34,41). We translated the animal studies to humans and found Nef signature sequences associated with PAH (2). Altogether, these results led us to propose a role for Nef in the development of HIV-PAH.

The current literature portraits non-human primates as animal models for SIV(HIV)-associated pulmonary disease by reporting the ultimate pathogenic pulmonary outcomes of the research efforts; however, the features in the actual disease progression remain poorly described. Therefore, we sought to gain further insights into inflammatory marker production and vascular remodeling in rhesus macaques in the context of SHIV*nef* infection. Herein, we show the spectrum of mild to aggressive pulmonary vascular disease in SHIV*nef*-infected macaques. Furthermore, we examined whether cytokines previously implicated in PAH were present in this animal model. We found that macaques infected with SHIV*nef* resulted in development of pulmonary vascular lesions and expressed a gene program characteristic of pathologic cardiac hypertrophy frequently seen in hearts of patients with PAH. Furthermore, these studies demonstrated alterations in cytokine expression consistent with other forms of PAH, highlighting the long-standing utility of this model to dissect pathogenic mechanisms.

Materials and Methods

Inoculation and care of rhesus macaques

Juvenile (3-year old) male rhesus macaques (*Macaca mulatta,* Mmu) were purchased from a D retrovirus-free and SIV-free colony at the California Regional Primate Research Center (CNPRC, $n=6$) and the New England Primate Research Center (NEPRC, $n=6$); we used two different centers due to contractual reasons. Parentage and ancestry analyses were performed as described by Kanthaswamy *et al.* (26). All animals at NEPRC and CNPRC were pure Indian rhesus, except animal CNPRC 6, which was confirmed as a Chinese-Indian hybrid. Animals were inoculated intravenously with 500 μL of cell-free SHIVnef_{SF33A} (32). Figure 1 depicts the natural history of the SHIV*nef* virions used for infection. The chimeric SHIV*nef* SF_{33A} used to infect our NEPRC monkeys was passaged once *in vivo*, upon recovery from a macaque that died of simian AIDS at 53 weeks postinfection (32). On the other hand, the $SF33_{A2}$ virus used to infect the CNPRC group was passaged twice. All animals remained antiretroviral drug-naïve throughout this study. The animals were cared for in accordance with the standards of the American Association for Assessment and Accreditation of Laboratory Animal Care. Animals were monitored daily for hydration, appetite, weight loss, temperature, diarrhea, behavioral changes, activity level, and opportunistic infections and euthanized by intravenous overdose of sodium pentobarbital when signs of immunodeficiency, that is, 15% weight loss in 2 weeks, ~7% dehydration, persistent leukopenia, presence of opportunistic infections, or abdominal lesions were detected.

Histopathology

Tissues collected at necropsy were formalin-fixed and paraffin-embedded or flash frozen in OCT. Lung serial sections lungs were stained with hematoxylin and eosin, as per standard protocols, scanned digitally using the Aperio ScanScope software (Vista, CA), and examined by two experienced pathologists in a blinded fashion. For analyses using immunofluorescence microscopy, formalin-fixed paraffin-embedded serial lung sections were stained with fluorescently labeled antibodies as follows: Nef (mouse monoclonal antibody; Advanced BioTech, Eldersburg, MD), biotinylated goat anti-mouse, and streptavidin-Texas Red antibody (Molecular Probes, Frederic, MD). Sections were washed and incubated with 10% donkey serum and stained for lymphocytes (rabbit anti-CD3; Dako), stem cells (rabbit anti-CD34; Abcam, Cambridge, MA), macrophages (rabbit anti-CD163; Sigma, St. Louis, MO), or smooth muscle (rabbit anti-smooth muscle actin; Abcam). After incubation with primary antibodies, sections were stained with anti-rabbit AF647 (Molecular Probes). In addition, endothelial cells were labeled with von Willebrand factor antibody conjugated to FITC (GeneTex, Irvine, CA). Coverslips were mounted using VECTASHIELD HardSet mounting media with DAPI (Vector Labs, Burlingame, CA). Isotype controls were also included. The pixel intensities were measured in grayscale images and a threshold was set for all images using a common factor of the mean pixel intensity. The threshold was used to calculate mean fluorescence intensities using Image J processing program; intensities from three images captured for each macaque were averaged and plotted.

Cardiac ventricle gene expression

Total RNA from the left or right ventricles was individually isolated from four SHIV*nef*-infected macaques and one SIV-infected control with TRIzol reagent (Life Technologies) according to manufacturer's specifications. First-strand cDNA

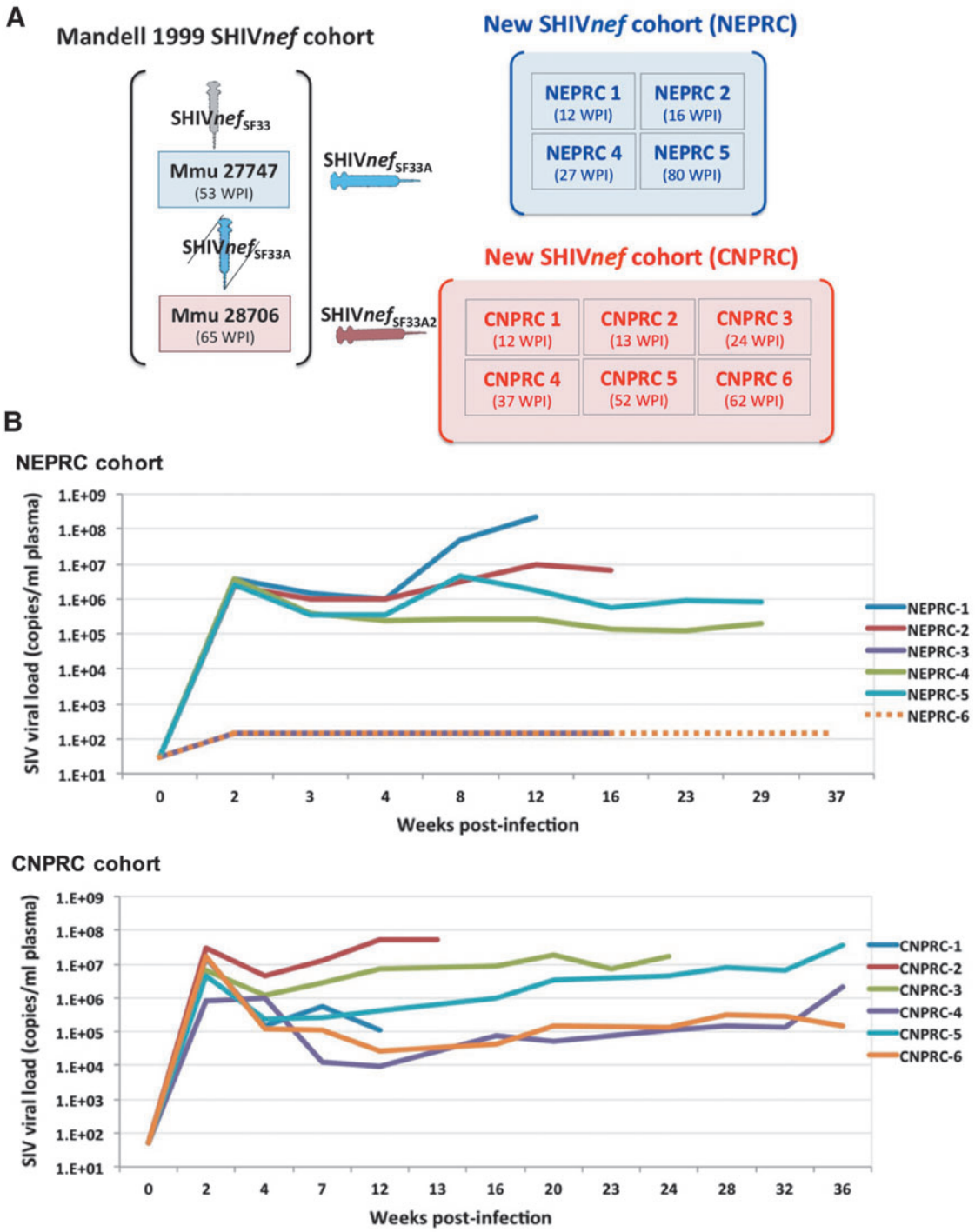

FIG. 1. **(A)** History of the *in vivo* passages of the SHIV*nef* chimeric viruses used to inoculate rhesus macaques. Mandell *et al.* first reported simian AIDS in rhesus macaques (*Macaca mulatta,* Mmu) infected with chimeric SHIV*nef* viruses expressing HIV nef in the SIVmac239 genetic backbone. The uncloned virus recovered from their animal Mmu 27747, designated as ''SHIVnef_{SF33A}'' was used to infect their Mmu 28706 and our new cohort of four rhesus macaques housed at the NEPRC (serial passage 1); two uninfected macaques (NEPRC 3 and 6) served as controls (not shown). The uncloned virus recovered from Mmu 28706 was used to infect our cohort of six rhesus macaques at CNPRC (serial passage 2). Each rectangle represents a macaque, whose ID is indicated. Animals were euthanized at the WPI indicated in *parentheses*. **(B)** Plasma SIV viral load in macaques inoculated intravenously with chimeric SHIV*nef*. Four rhesus macaques were inoculated with SHIV*nef* SF33A at NEPRC. Two uninfected rhesus served as negative controls: one was euthanized after the second experimental macaque was necropsied; the second uninfected control was euthanized after the fourth experimental monkey and monitored from baseline up to 37 weeks PI. Plasma viral load of infected macaques were measured for 29 weeks only. Six rhesus macaques were infected with SHIV*nef* SF33A2 at CNPRC. Each *colored line* represents data from each macaque, at the indicated weeks postinfection. SIV viral loads are in a logarithmic scale. NEPRC, New England Primate Research Center; CNPRC, California National Primate Research Center; SIV, simian immunodeficiency virus; WPI, weeks postinfection.

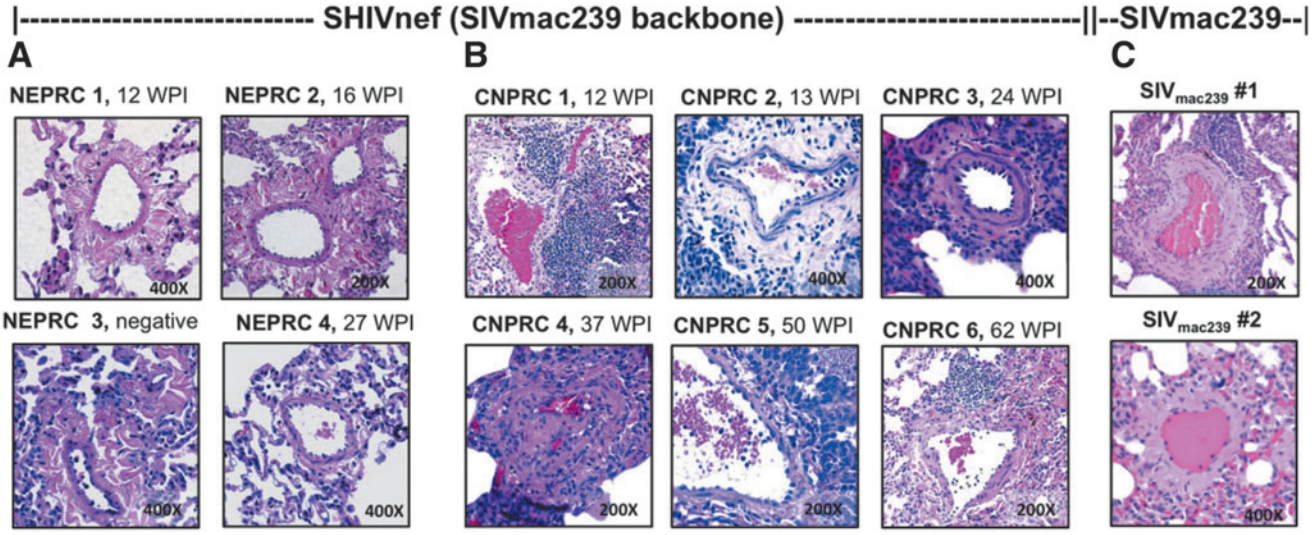

FIG. 2. Pulmonary vasculature in rhesus macaques infected with SHIV*nef* chimeric virions and parental SIV_{mac239}. Paraffin-embedded sections from the lungs of rhesus macaques infected with $SHIVnef_{SF33A}$ (NEPRC, **A**), $SHIVnef_{SF33A2}$ (CNPRC, **B**), or SIV_{mac239} (**C**) were stained with hematoxylin and eosin and examined for vascular pathologies by two independent pathologists. SHIV*nef*-infected monkeys in the NEPRC cohort showed evidence of mild pulmonary vascular pathology (mostly adventitial but no medial thickening) with inflammation (**A**). In contrast, the CNPRC animals presented evidence of pulmonary vascular remodeling (**B**). Note that CNPRC 4 showed major remodeling, recanalized obstructive lesion at 37 WPI. In addition, we examined H&E-stained lung sections of two adult rhesus macaques, aged 11 and 14 years, infected with the parental $SIVmac_{239}$ for 78–81 weeks (elite controllers). Despite their advanced age relative to our juvenile monkeys, these animals exhibited mild pulmonary vascular pathology (**C**). Magnifications are shown for each image.

synthesis was performed using Superscript II reverse transcriptase and random hexamer primers as described previously (5,24). Expression of cardiac hypertrophy genes was quantified by real-time PCR.

Laboratory assessments and course of infection

Blood was drawn from monkeys anesthetized with an intramuscular injection of ketamine hydrochloride at various time points (5 mL peripheral blood) for routine SIV viral load testing (measured by real-time TaqMan PCR, with a sensitivity of $\sim$50 copies/mL), complete blood counts (CBC), and peripheral blood lymphocyte subset counts by flow cytometry. Values were compared to normal reference values (7,17); median values relative to reference intervals were used to define hematopathologies. We measured cytokine and chemokine levels in plasma using Luminex multiplex microbead immunoassay arrays, as described (16,20). The Luminex 20-plex bead combination included in-house reagents and commercial beads purchased from Life Technologies (Frederic, MD), EMD Millipore (Billerica, MA), and R&D Systems (Minneapolis, MN). All animals remained antiretroviral drug-naïve throughout this study.

Inflammatory gene expression profiles

Cell-associated total RNA was extracted from flash-frozen lung tissues with Qiagen miRNeasy Mini Kit. The quality of the extracted RNA was assessed in an R6K ScreenTape (Agilent Technologies, Santa Clara, CA). The cDNA was synthesized using the RT^2 First Strand Kit; reactions for quantitative PCR were prepared with the RT^2 SYBR Green Fluor qPCR Master Mix Kit (SABiosciences, Valencia, CA). Samples were

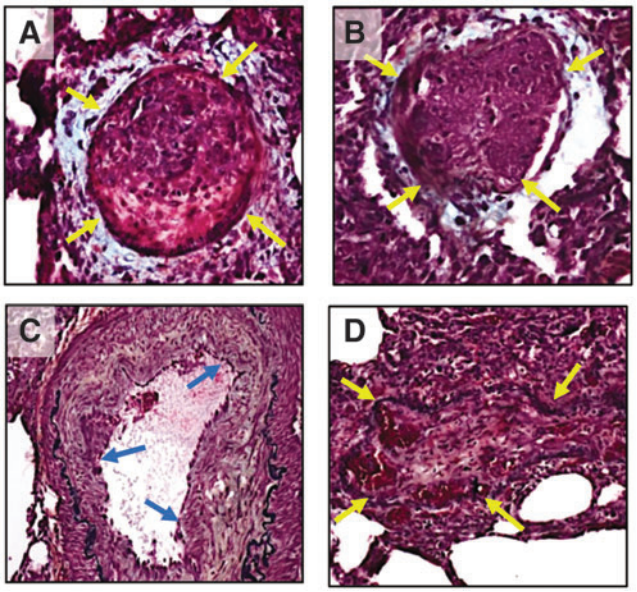

FIG. 3. Pentachrome staining in plexiform lesions in the pulmonary vasculature of rhesus macaque CNPRC 4 infected with SHIV*nef*. Paraffin-embedded sections of the lungs of macaque CNPRC 4 were stained with Movat's pentachrome (**A–D**). Note that this monkey exhibited major remodeling with obstructive lesions at 37 WPI. *Arrows* indicate obliterated lumena. Note that the obliterative lesions are composed mostly of fibrin (*bright red*) and muscle (*red*) surrounded by mucin (*light blue* in **A, B**). Elastic fibers are shown in *black* (**C, D**). Collagen/reticular fibers are shown in yellowish color in (**C**). All images were captured at 200$\times$ magnification.

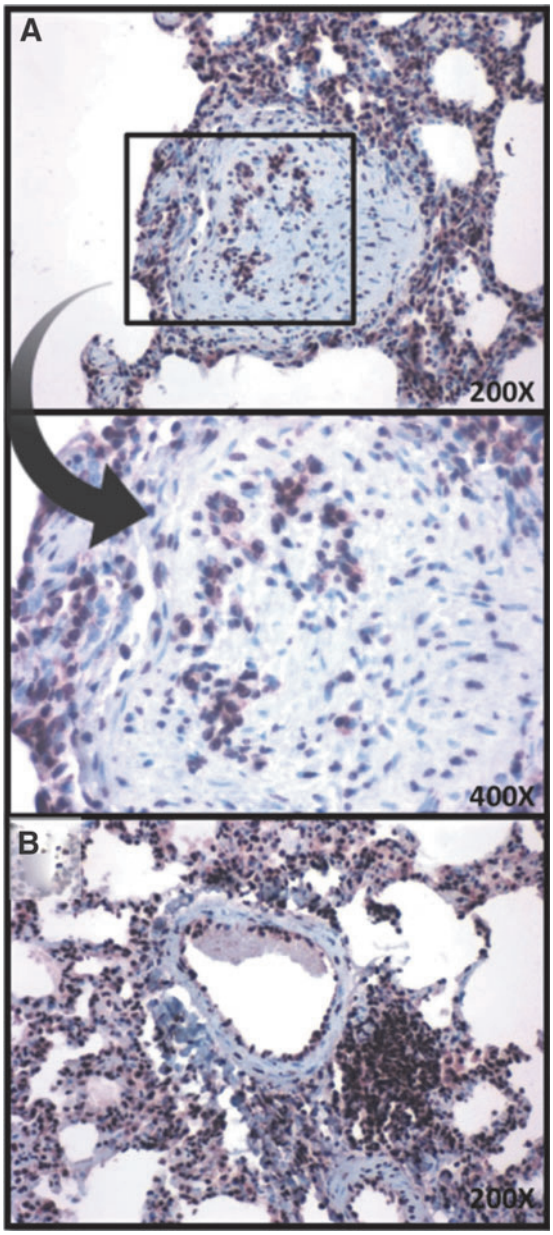

FIG. 4. Detection of HIV Nef protein in the pulmonary vasculature of a SHIV*nef*-infected macaque exhibiting pulmonary vascular lesions after 37 weeks postinfection. Formalin-fixed paraffin-embedded lung tissue of macaque CNPRC 4 was stained with anti-Nef antibody and counterstained with hematoxylin **(A, B)**. The area enclosed by the *box* **(A)** is shown at higher magnification (indicated by *arrow*). Magnifications are shown for each image.

amplified using the PCR targeted array for Rhesus Macaque Inflammatory Cytokines & Receptors as per manufacturer protocols. The housekeeping genes beta-2-microglobulin and hypoxanthine-guanine phosphoribosyltransferase-like were used for normalization. Gene expression was determined via the $\Delta\Delta C_t$ method; fold changes were calculated based on difference in gene expression between SHIV*nef*- and $SIVmac_{239}$-infected macaques. Gene expression results were queried for potential biological relevance using the Ingenuity Pathway Analysis (IPA) software (Qiagen, www.ingenuity.com).

Bioinformatics analysis

The fold change data for the 84 genes compared in the SHIV*nef* versus SIVmac239 infections were uploaded into IPA (www.ingenuity.com) and used to predict potential pathways affecting these genes. IPA uses a Fisher's exact test to identify over-represented connected biological units in a defined set of genes, which can include pathways, cellular functions, or known targets of regulatory genes. In some cases, a confidence score, or z-score, can be made on the activation state of the pathway or upstream regulator based on the expression pattern of the associated genes (28). The activation z-score is used to infer likely activation states of upstream regulators based on comparison with a model that assigns random regulation directions; regulators with higher z-scores have more evidence of activation, while regulators with lower z-scores have more evidence of inhibition over the random model.

Results

*SHIV*nef*-infected rhesus macaques show variable infection dynamics after passage* in vivo

In this study, animals at NEPRC were infected with chimeric $SHIVnef_{SF33}$ after one passage *in vivo*, while the CNPRC monkeys were infected with $SHIVnef_{SF33}$ after two serial passages, as indicated in Figure 1A. Baseline and longitudinal measurements of plasma SIV RNA confirmed productive infection in all infected animals. Peak plasma viral load during acute infection was observed at 2 weeks postinoculation. Macaques in the CNPRC cohort trended to have higher viral loads during the acute phase (mean, 1.24×10^7 copies/mL) compared to animals at NEPRC (mean, 3.05×10^6 copies/mL, $p = 0.0952$) (Fig. 1B). Survival times postinfection in the CNPRC group ranged from 12 to 62 weeks, with median 30.5 weeks and mean 33 weeks (95% CI: 11.7–54.3). In the NEPRC group, the survival times ranged from 12 to 80 weeks, with median 21.5 weeks and mean 34 weeks (95% CI: −16.3 to 83.8). Differences in survival between the cohorts were not statistically significant different ($p = 0.7679$, Log-rank Mantel-Cox test).

*Pulmonary vascular remodeling in SHIV*nef*-infected macaques*

SHIV*nef*-infected monkeys in the NEPRC cohort showed mild adventitial pulmonary vascular thickening with inflammatory infiltrates (see representative images in Fig. 2A). In contrast, the CNPRC animals (Fig. 2B) showed significant pulmonary vascular remodeling. Specifically, pathological remarks in the first animal, CNPRC 1, included predominant bronchial associated lymphoid tissue, medial hypertrophy, prominent lymphocytic infiltration, and vascular remodeling at 12 weeks postinfection (WPI). Macaque CNPRC 2 and 3 showed apoptotic bodies, presence of neutrophils, pneumonia, giant cells indicative of severe infection, and foci of lymphocyte infiltrations at 13 and 24 WPI. Macaque CNPRC 4 showed major remodeling, obstructive recanalized lesions, plump endothelial cells, intravascular thrombotic bodies, medial hypertrophy, and plexiform lesions at 37 WPI; pentachrome staining identified fibrin and muscle within the lesions (Fig. 3). HIV Nef protein was detected in the lesions of this animal by immunohistochemistry (Fig. 4). No vascular

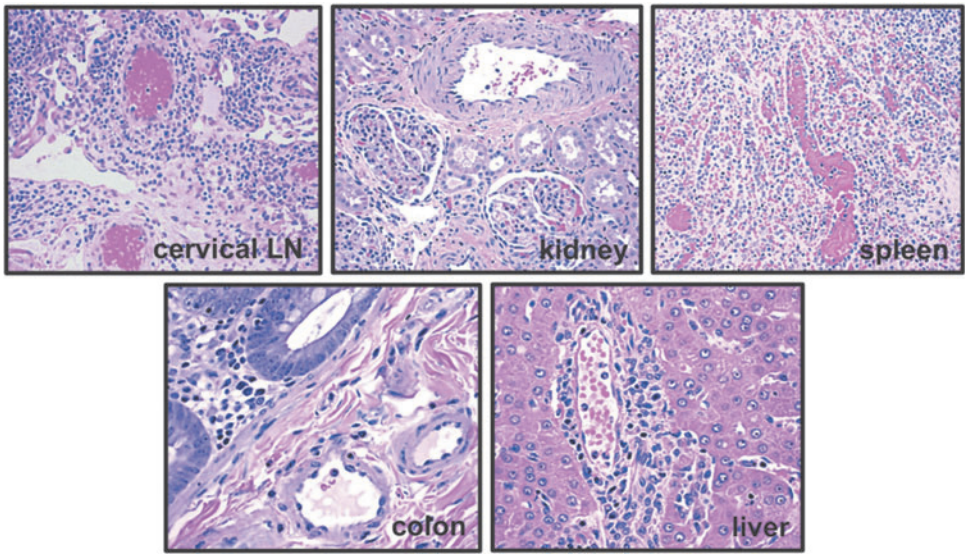

FIG. 5. Extra-pulmonary vasculature in macaque CNPRC 4 exhibiting significant pulmonary vascular remodeling. Animal CNPRC 4 showed complex obliterative lesions in the pulmonary vasculature at necropsy at 37 weeks postinfection (see Fig. 3B). Paraffin-embedded sections of the vasculature in cervical lymph node, kidney, spleen, colon, and liver of this animal were stained with hematoxylin and eosin and examined. No significant vascular remodeling was observed in any of these organs, suggesting that SHIV*nef* infection leads to pulmonary-specific vascular remodeling. All images were captured at a 200× magnification.

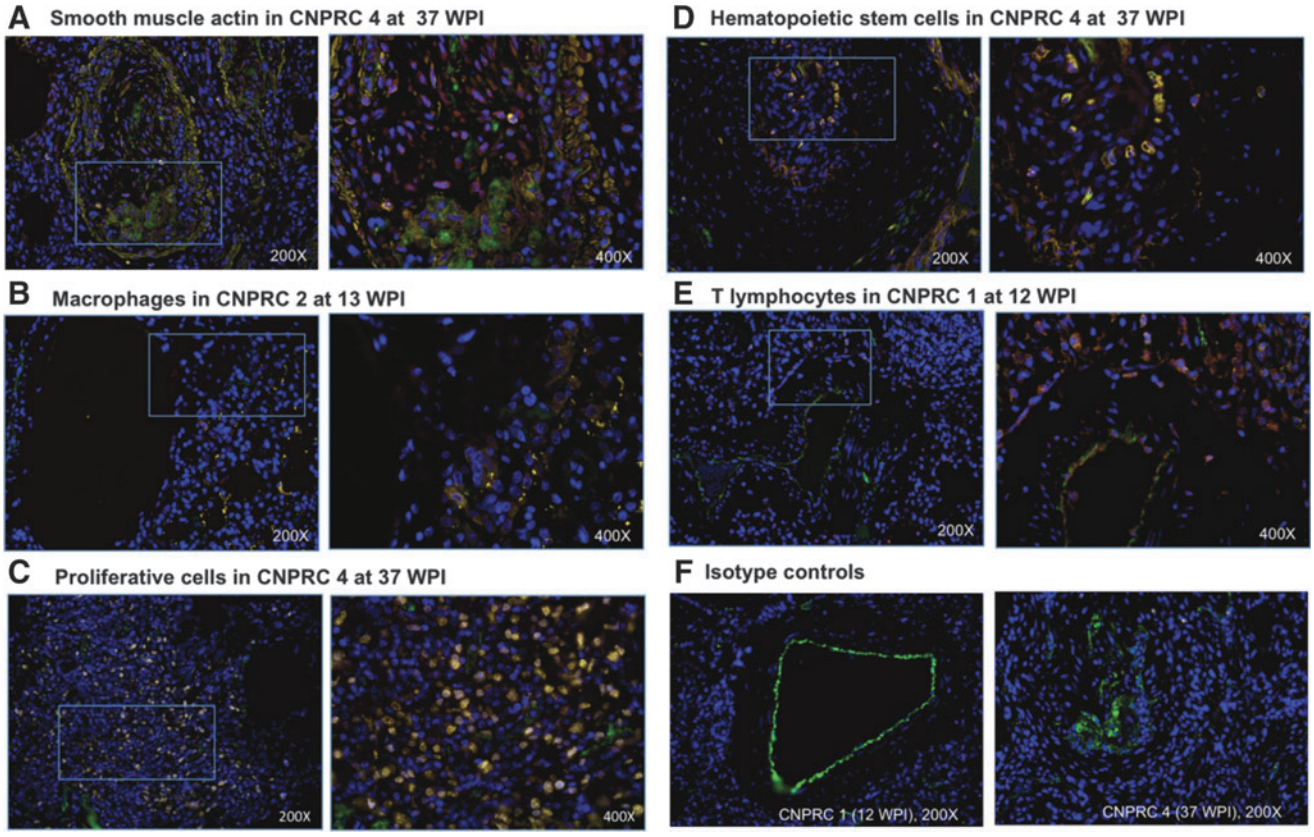

FIG. 6. Phenotypic characterization of cells in the pulmonary vasculature of rhesus macaques infected with SHIV*nef*. Immunofluorescent staining for smooth muscle actin (*yellow*, **A**), macrophages (CD163 in *yellow*, **B**), proliferative cells (Ki-67 in *yellow*, **C**), stem cells (CD34 in *yellow*, **D**), and T lymphocytes (CD3 in *yellow*, **E**). Each staining was multiplexed with staining for endothelial cells (Von Willebrand factor, *green*), Nef (*red*), and nuclei (*blue*). Macaques with statistically significant higher immunofluorescence are shown (see Fig. 6 for quantification results); macaque ID and weeks postinfection (WPI) are shown on *top* of each panel. The *insets* indicated by rectangles on the *left* are shown to the *right*, in higher magnification. Panel **F** shows the isotype controls (mouse IgG, *yellow*) multiplexed with staining for endothelial cells and nuclei. All figures show merged images. Magnifications are shown for each figure.

lesions were found in the spleen, lymph nodes, kidney, liver, and colon, suggesting pulmonary artery-specific pathology (Fig. 5). Despite the severe pulmonary vascular remodeling observed in animal CNPRC4, very little inflammatory cell infiltration was seen in the lungs compared to its mates. CNPRC 5 showed prominent alveolar proteinosis, which made it difficult to identify lung abnormalities. Lastly, CNPRC 6 showed prominent lymphoid follicles indicative of exuberant bronchiolitis at 62 WPI (Fig. 2B). Because aging is known to promote remodeling of the pulmonary vasculature, with an increase in muscle content of the pulmonary artery and stiffness (45), we examined archival material consisting of H&E-stained lung sections of two adult rhesus macaques, aged 11 and 14 years infected with the parental SIVmac$_{239}$ for 78–81 weeks and designated as old, long-term nonprogressors. Despite the advanced age of the SIVmac239-infected monkeys compared to our juvenile SHIV*nef*-infected macaques, the former exhibited adventitial pathology with inflammation without vascular lesions (Fig. 2C).

*Immunophenotypic characterization of cells in the lungs of SHIV*nef*-infected macaques*

Given the evidence of pulmonary vascular remodeling in the SHIV*nef*-infected macaques from the CNPRC group, we characterized the pulmonary vascular cells. Lung tissue sections were stained with fluorescent-labeled antibodies to T lymphocytes (CD3), macrophages (CD163), smooth muscle actin, hematopoietic stem cells (CD34), or proliferating cells (Ki-67) multiplexed with markers for endothelial cells (von-Willebrand factor), Nef, and nuclei (DAPI). Notably, there were numerous Ki-67 positive cells

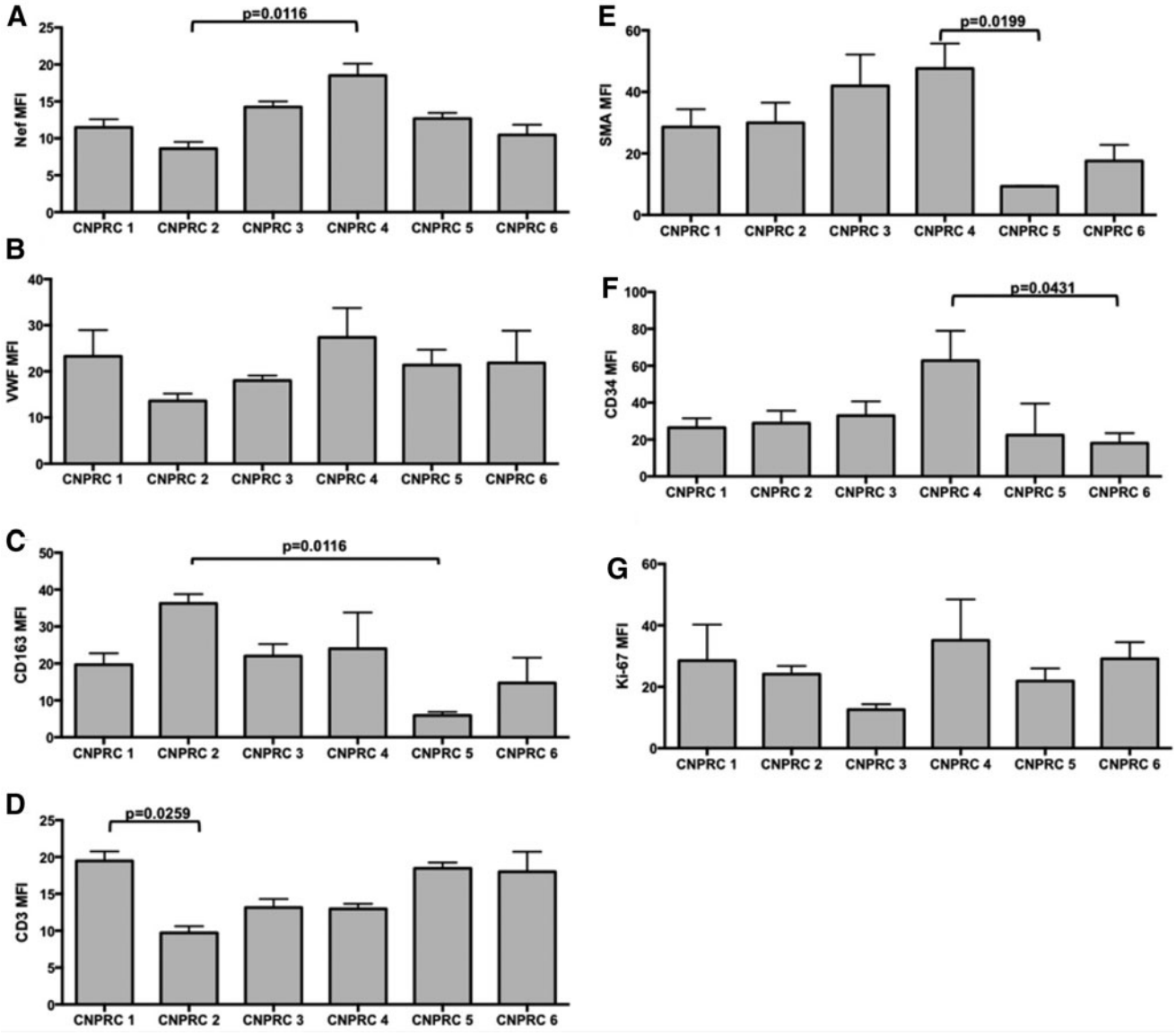

FIG. 7. Quantification of immunofluorescent signals in the pulmonary vasculature of rhesus macaques infected with SHIV*nef*. Immunofluorescent signals for HIV Nef **(A)**, von Willebrand factor for endothelial cells **(B)**, CD163 for macrophages **(C)**, CD3 for lymphocytes **(D)**, SMA for smooth muscle actin **(E)**, CD34 for stem cells **(F)**, and Ki-67 for proliferation **(G)** were quantified in Image J and analyzed statistically. The adjusted *p*-values from the Kruskal–Wallis test followed by Dunn's multiple comparison tests are shown for the significant quantifications. MFI, mean fluorescence intensity.

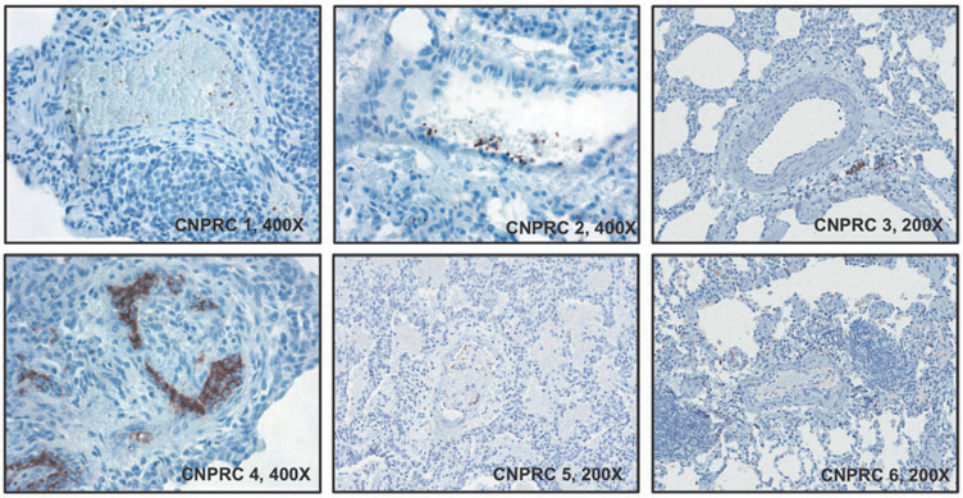

FIG. 8. Immunohistochemical analysis of microthrombi in the pulmonary vasculature of SHIV*nef*-infected rhesus macaques. Intravascular staining of the platelet marker CD61, microthrombi. CD61 sections was detected by immunoperoxidase (*brown*) and counterstained with hematoxylin. Note the staining pattern in CNPRC 4, suggestive of intravascular platelet aggregates. Magnifications are shown for each image.

in the pulmonary plexogenic lesion in animal CNPRC 4 (see representative images in Fig. 6). Quantification of immunofluorescent signals for cellular markers in each animal (Fig. 7) shows that macaque CNPRC 1 (12 WPI) had the highest CD3 ($p=0.0259$) and CNPRC 2 (13 WPI) had the highest CD163 levels ($p=0.0116$) compared to their mates. The macaque with exuberant pulmonary vascular remodeling at 37 WPI (CNPRC 4) had the highest smooth muscle actin ($p=0.0199$), CD34 ($p=0.0431$), and Nef ($p=0.0116$). There was no significant difference in signals for Ki-67 or Factor VIII among the CNPRC macaques. Because *in situ* thrombosis plays a pathophysiologic role in PAH, we analyzed the platelet marker CD61 in the pulmonary vasculature. Immunohistochemical analyses showed higher intravascular CD61 staining in animal CNPRC 4 (Fig. 8), suggesting intrapulmonary platelet aggregation.

Cardiac hypertrophy markers

We measured cardiac hypertrophic gene expression in four CNPRC macaques compared to one $SIVmac_{239}$-infected control. Cardiac mRNA gene expression changes associated with pathological hypertrophy include changes in the relative expression of the α and β myosin heavy chain (MHC) isoforms where α is repressed, decreased expression of sarco(endo)-plasmic reticulum Ca2+-ATPase (SERCA), and increased expression of atrial natriuretic peptide (ANP), and brain natriuretic peptide (BNP). Consistent with the generalized induction of pathologic cardiac hypertrophy, we found that expression of the natriuretic peptide BNP was increased in ventricles of all CNPRC animals examined while ANP was upregulated in LVs of all experimental animals but in the RV of only CNPRC4. α-MHC RNA was repressed in all CNPRC samples with the exception of the RV of CNPRC4. Beta Adrenergic gene expression also showed a generalized pattern of repression in CNPRC animals when compared with controls with the exception of CNPRC4 where the Beta 2 AR expression was increased. The relative abundance of SERCA was also decreased in all of the SHIV*nef* macaques relative to the control. These results are shown in Figure 9.

*Hematopathologies in SHIV*nef*-infected macaques in the CNPRC cohort*

CBC collected longitudinally in all macaques were compared to reference CBC values for male rhesus macaques (7,17). For most end points, the median CBC values remained within normal levels in the NEPRC macaques throughout the course of the study. We found persistent lymphopenia (defined as low lymphocyte counts relative to reference values) in the animal euthanized at 27 WPI (NEPRC4). On the other hand, several blood cell abnormalities were found in the CNPRC animals. Specifically, most of the CNPRC monkeys (CNPRC 2,3, and 4) had significantly low hemoglobin and hematocrit values compared to their SHIV*nef*-infected mates, suggesting anemia. The animal euthanized at 37 WPI (CNPRC 4) also had significant neutrophilia (median 10230 cells/μL, 95%CI: 7826,18055), with persistent lymphopenia (median 1915 cells/μL blood, 95%CI: 1137,3101) and a striking thrombocytosis (high number of platelets (median 4.58×10^5 cells/μL, 95%CI: 3.25×10^5, 5.31×10^5) compared to the other SHIV*nef*-infected macaques at CNPRC. These hematopathologic findings are shown in Table 1 and in Figure 10.

Furthermore, we compared the CBC values between the two cohorts (excluding uninfected controls) and found that the SHIV*nef*-infected monkeys in the NEPRC were significantly more lymphocytopenic than their CNPRC counterparts ($p=0.0046$, Mann–Whitney Test). In addition, animals in the CNPRC group had significantly lower RBC, hemoglobin, and hematocrit values than the NEPRC animals ($p<0.0001$, Student's t test). No statistically significant differences were observed in white blood cell counts or platelets between the two cohorts (Fig. 11 and Table 2). Altogether, these data suggest a worse course of disease in the CNPRC animals infected with chimeric

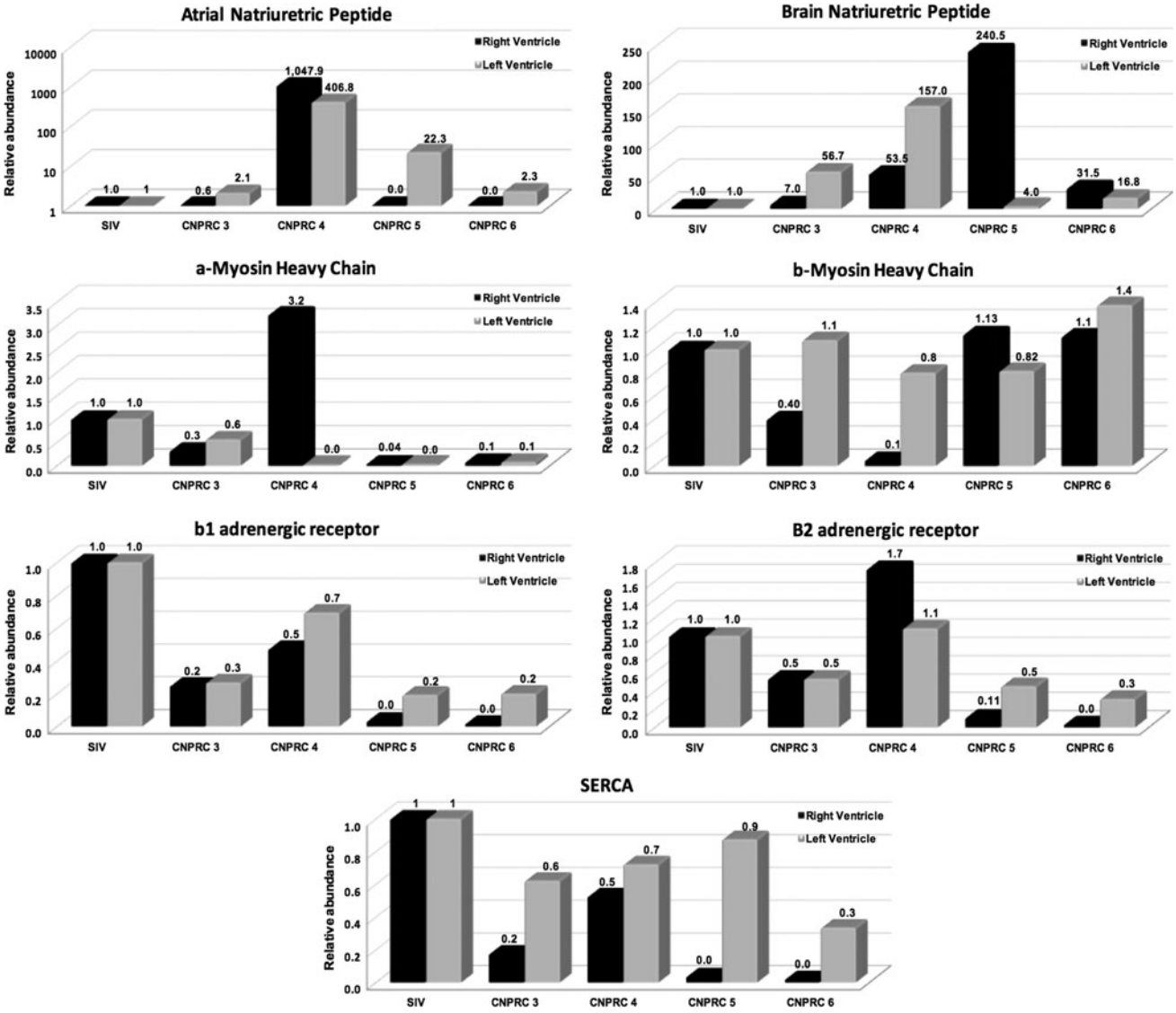

FIG. 9. Cardiac hypertrophic gene expression in SHIV*nef*-infected macaques. Total RNA from the *right* and *left* ventricle was extracted and analyzed by real-time PCR. We found that genetic expression of ANP, α-MHC, and β2 adrenergic receptors were evidently increased in the *right* ventricle of macaque CNPRC 4, In addition, *left* ventricular gene expression in macaque CNPRC 4 switched from α and β isoform of MHC. Ventricular BNP was also increased in CNPRC 4 and 5. The relative abundance of SERCA was decreased in SHIV*nef* macaques relative to the control. All these changes in gene expression are associated with ventricular dysfunction and hypertrophy. SERCA, sarco(endo)plasmic reticulum Car^{2+} ATPase; ANP, atrial natriuretic peptide; BNP, brain natriuretic peptide.

SHIV*nef* passaged twice than the NEPRC monkeys infected with SHIV*nef* virus passaged only once.

*Inflammatory biomarkers in plasma and lungs of SHIV*nef*-infected rhesus*

Plasma cytokines were measured in six CNPRC SHIV*nef* and four $SIVmac_{239}$-infected rhesus. Group-specific intercepts and slopes for weeks postinfection were estimated from a linear mixed-effects model for each of the tested cytokines (Table 3). Compared to the SIV group, the average cytokine value was significantly higher in the SHIV*nef* group for cytokines IL-12 ($p = 0.0002$) and granulocyte macrophage colony stimulating factor-2 (GM-CSF, $p < 0.0001$), and significantly lower in the SHIV*nef* group for soluble CD40 ligand (sCD40 L, $p = 0.0002$), monocyte chemotactic protein-1 (CCL-2/MCP-1, $p = 0.0063$), and growth-related oncogene alpha (CXCL-1/GRO-a, $p = 0.0038$, Fig. 12). The relationship between time and cytokine was not different between the two groups for any of the inflammatory cytokines.

We next analyzed inflammatory gene expression in the lungs of the six CNPRC SHIV*nef*-infected macaques compared to two $SIVmac_{239}$-infected rhesus macaques by PCR array. We found that the SHIV*nef*-infected macaques had approximately six-fold decrease in CD40 L and approximately three-fold increase in interleukin 6, a four-fold increased CCL2/MCP-1 and CCL20/MIP3a, and a ~12-fold increase in CCL23 (Table 4). All the gene expression data were

Table 1. Hematologic Abnormalities in SHIV*NEF*-Infected Macaques

	NEPRC			
	NEPRC 1, (12 WPI)	*NEPRC 2, (16 WPI)*	*NEPRC 4, (27 WPI)*	*NEPRC 5, (80 WPI)*
White blood cells	→	↓	→	→
Red blood cells	→	→	→	→
Hemoglobin	→	→	→	→
Hematocrit	→	→	→	→
Platelets	→	↓	→	↓
Lymphocytes	→	↓	↓ ($p<0.05$)	→

	CNPRC					
	CNPRC 1, (12 WPI)	*CNPRC 2, (13 WPI)*	*CNPRC 3, (24 WPI)*	*CNPRC 4, (37 WPI)*	*CNPRC 5, (50 WPI)*	*CNPRC 6, (62 WPI)*
White blood cells	→		→	→	→	↓
Red blood cells	→	↓	↓	↓	→	↓ ($p<0.05$)
Hemoglobin	↓	↓ ($p<0.01$)	↓ ($p<0.001$)	↓ ($p<0.01$)	→	↓
Hematocrit	↓	↓ ($p<0.01$)	↓	↓ ($p<0.01$)	→	↓ ($p<0.01$)
Platelets	↑	→	↓	↑	↓	↓
Lymphocytes	→	→	→	↓ ($p<0.001$)	→	↓
Mean cell hemoglobin	↓ ($p<0.01$)	↓ ($p<0.01$)	↓	↓ ($p<0.001$)	→	→
Neutrophils	↑	↓	↑	↑ ($p<0.01$)	→	↓
Monocytes	→	→	→	↑	→	→
Eosinophils	↑	→	→	↑	→	→

Longitudinal complete blood count (CBC) in SHIV*nef*-infected macaques at NEPRC (*top panel*) and CNPRC (*bottom panel*). Macaque IDs are shown, with the times postinfection in parenthesis. CBC data were analyzed relative to normal CBC values in male Rhesus macaques (Gill *et al.* 2012 and Chen *et al.* 2009). Values were categorized as blood cell abnormalities if the median values exceeded the normal intervals (*up arrows*) or were below the normal intervals (*down arrows*). Median values within the normal intervals are shown as *horizontal arrows*. Data were analyzed by one-way ANOVA with Dunn's multiple comparison tests to compare CBC values of each macaque with the rest of his mates. *p*-Values were determined with Gaussian approximations and are shown only for statistically significant CBC values. Statistical significance was set at $p<0.05$.

NEPRC, New England National Primate Research Center; CNPRC, California National Primate Research Center; WPI, weeks postinfection; SHIV*nef*, chimeric simian-human immunodeficiency virus containing HIV nef.

analyzed using the IPA software to identify potential transcription effectors in the context of SHIV*nef* infection. Relative to SIVmac239, we found the regulators bone morphogenetic protein-2 (BMP-2) and the transcription factor RelB were predicted to be the most inhibited and activated with SHIV*nef* infection, respectively, based on the direction of expression of their target genes (Fig. 13).

Discussion

Herein, we present the first comprehensive examination of pulmonary vascular changes and associated biomarker alterations in two separate cohorts of SHIV*nef*-infected macaques. This study confirms and extends our previous work demonstrating pulmonary vascular lesions consistent with HIV-PAH in rhesus macaques infected with SHIV*nef*, and that these lesions are not seen in animals infected with parental SIVmac239.

An observation derived from these studies is that the CNPRC animals infected with SHIV*nef* virions serially passaged twice had higher viral loads during the acute phase of infection, lower viral set points, faster progression to simian AIDS, and worse pulmonary vascular phenotypes than the animals infected with virus passaged only once. Bioinformatics sequence analyses are underway to elucidate whether virus passaging introduced mutations that translated to severe pulmonary disease in macaques. We further demonstrate that SHIV*nef* macaques exhibit cardiac hypertrophy and changes in plasma and lung cytokines consistent with PAH. Collectively, these data suggest that the SHIV*nef* rhesus macaque model recapitulates many aspects of HIV-PAH and its usefulness to further dissect the mechanisms that promote pulmonary vascular remodeling.

We noted vascular remodeling in the pulmonary vasculature but not in extra-pulmonary tissues. Consistent with our previous studies, we detected Nef within the plexiform lesions but the presence and/or abundance of Nef in non-pulmonary tissues and whether there is a correlation with presence/absence of vascular remodeling remains to be elucidated. We also noted differences in lung histopathology between the two cohorts of SHIV*nef*-infected rhesus macaques. The characteristic histopathology of PAH includes excessive proliferation of smooth muscle cells and endothelial cells to the point of lumen obliteration, with perivascular inflammatory cell infiltrates and intravascular thrombosis (1,3,39,46). While the NEPRC cohort showed mostly adventitial pulmonary vascular changes, the SHIV*nef*-infected macaques at CNPRC featured severe pulmonary artery-specific remodeling, including perivascular inflammatory cell infiltrates, medial hypertrophy, and obstructive plexiform lesions, and intravascular thrombosis particularly in macaque CNPRC 4. Histological and immunophenotypic characterization of cells in the lungs of SHIV*nef*-infected monkeys as a function of time suggest that once the plexiform lesions form, there is no

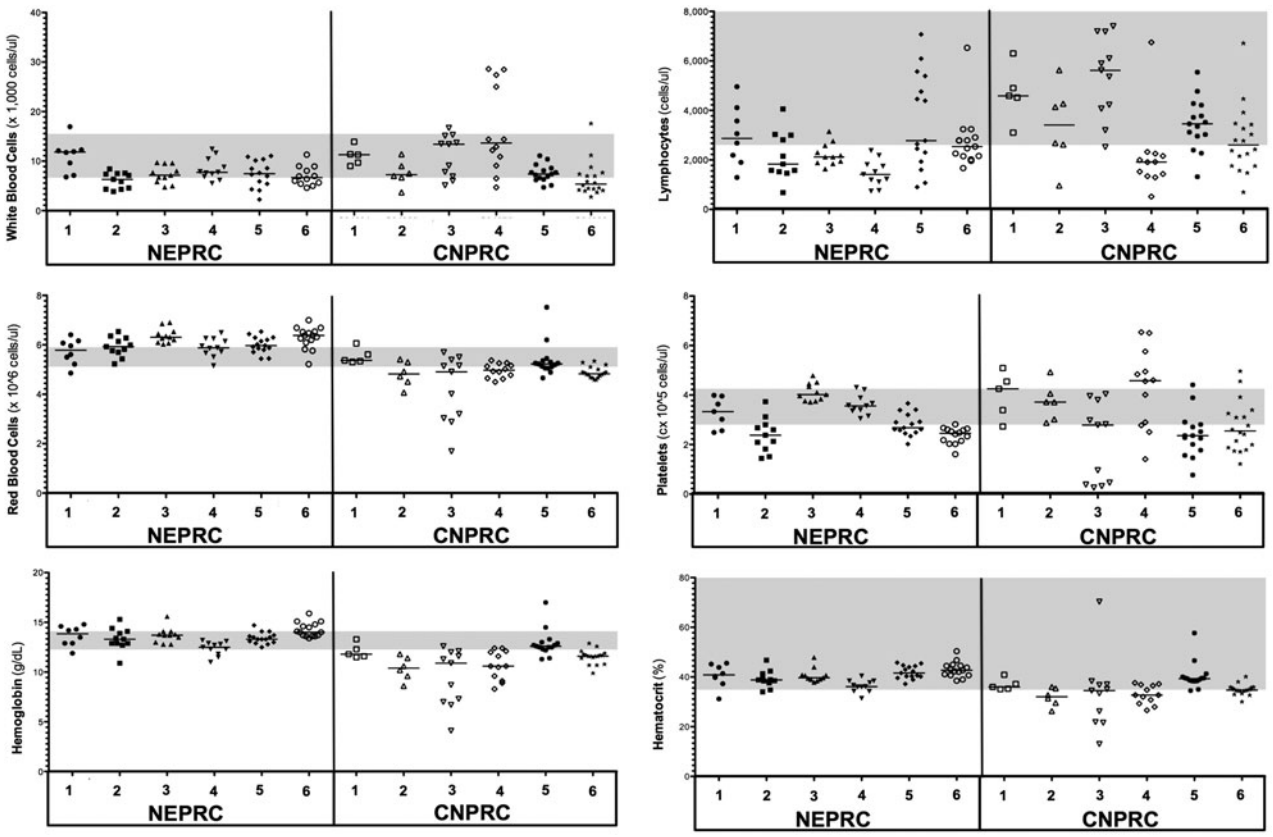

FIG. 10. Hematologic abnormalities in SHIV*nef*-infected macaques. Longitudinal CBC were measured in SHIV*nef*-infected macaques at NEPRC and CNPRC and analyzed relative to normal CBC values in male Rhesus macaques (Gill *et al.* 2012 and Chen *et al.* 2009); normal reference intervals are *shaded* in *gray*. Hematologic parameters are shown in the *y*-axes; macaque IDs are shown in the *x*-axes. Each *symbol* represents independent data points collected for each macaque; the *horizontal line* indicates the median value. Blood cell abnormalities were defined if the median CBC values exceeded or were below the normal reference values (*gray shaded* areas). CBC, complete blood counts.

longer evidence of inflammation. Numerous proliferating cells were observed in the pulmonary plexogenic lesion in animal CNPRC 4, which aligns with early descriptions of HIV-PAH lesions (8). Consistent with our previous studies (33,34), our findings were exclusive to SHIV*nef*-infected macaques but not in $SIVmac_{239}$-infected monkeys, even after longer duration of SIV infection and advanced age. Based on pentachrome staining, it is noteworthy that the obliterative lesions in our SHIV*nef* model are rich in fibrin and muscle cells, while the lesions reported in other SIV models are characterized by collagen deposition (6,15,44). Therefore, the mechanisms at play in the formation of PAH-associated lesions in the SHIV*nef* and SIV models are most likely different. Moreover, although the SIV and SHIV models have contributed to the overall knowledge to the field of HIV-PAH, the fact that the various studies used different macaque species infected with different SIV/SHIV strains complicated by the multifactorial nature of pulmonary vascular remodeling and PAH may confound some of the conclusions.

Our animals remained antiretroviral drug naive throughout the course of the study and were humanely euthanized when signs of immunodeficiency were detected. Similar to human HIV disease, our macaques progressed to simian AIDS at different rates and therefore, were terminated between 12 and 62 WPI. This represents an inherent limitation in our study because the broad range in length of viral infection makes it difficult to compare vascular pathologies. Our studies were also limited by the lack of hemodynamic data for a conclusive diagnosis of PAH in the setting of SHIV*nef* infection. While increased pulmonary artery pressures have been already reported in infected macaques as early as 12 weeks postinfection (15), our histological and cardiac hypertrophy marker lines of evidence support the observation of pulmonary vascular remodeling with right ventricular hypertrophy. There was a generalized change in the expression of a number of cardiac-myocyte selective genes consistent with what has been described as the pathologic gene program (38,47) in the CNPRC animals examined. Specifically, there was an increase in expression of the natriuretic peptides, a repression of SERCA and Beta Adrenergic Receptor subtypes and a change in MHC isoforms favoring the β- over the α-isoform. Several blood cell abnormalities were also found in the CNPRC animals, including significant neutrophilia, anemia, and lymphopenia. Of note, macaque CNPRC 4 showed severe anemia with thrombocytosis with intrapulmonary thrombosis. Interestingly, small vessel thrombosis is a common finding in idiopathic PAH (3,4). Whether intravascular pulmonary thrombi developed *in situ* or by embolization remains an open area of investigation.

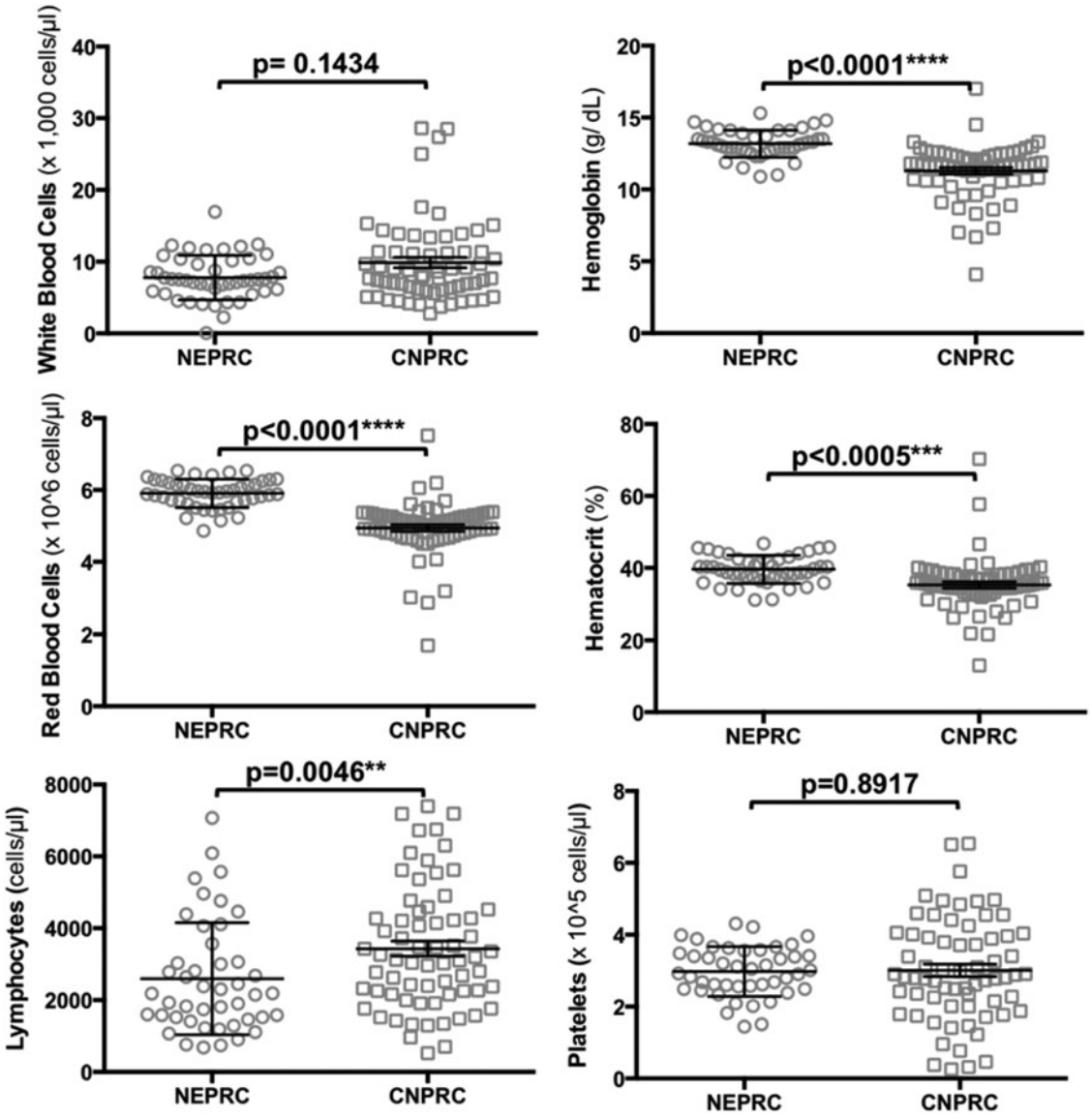

FIG. 11. Comparison of CBC values between SHIV*nef*-infected macaques in NEPRC and CNPRC. CBC were performed throughout the course of the infection with SHIV*nef*-infected macaques (4 NEPRC and 6 CNPRC animals). Each hematologic parameter is shown in the *y*-axis; each macaque group is indicated on the *x*-axis. Data are represented by scatter *dot plots* with *lines* at the mean with SEM. White blood cells and lymphocyte data were analyzed by nonparametric Mann–Whitney U tests; Student's *t*-tests were used to analyze the other parameters. *p*-Values are shown for each parameter analyzed.

TABLE 2. COMPARISON OF CBC VALUES BETWEEN SHIV*NEF*-INFECTED MACAQUES IN NEPRC AND CNPRC

	NEPRC			*CNPRC*			
CBC parameter	*Median*	*Mean*	*95% CI*	*Median*	*Mean*	*95% CI*	p-*Value*^{test}
White blood cells ($\times$1,000/µL)	7.46	7.92	6.87–8.71	8.10	9.88	8.42–11.35	0.1434,^{MWT}
Red blood cells ($\times 10^6$/µL)	5.93	5.91	5.80–6.03	5.05	4.95	4.76–5.13	<0.0001,^{STT}
Lymphocytes (cells/µL)	2180	2598	2130–3067	3120	3433	3014–3851	0.0045,^{MWT}
Hemoglobin (g/dL)	13.10	13.18	12.90–13.47	11.60	11.29	10.83–11.75	<0.0001,^{STT}
Hematocrit (%)	39.8	39.7	38.5–40.8	35.1	35.4	33.7–37.2	0.0005,^{STT}
Platelets ($\times 10^5$/µL)	2.97	2.98	2.77–3.19	2.82	3.01	2.66–3.36	0.8917,^{STT}

Complete blood counts (CBC) were performed throughout the course of the infection with SHIV*nef*-infected macaques. White blood cells and lymphocyte data were analyzed by nonparametric Mann–Whitney U tests; Student's *t* tests were used to analyze the other parameters. *p*-Values are shown for each parameter analyzed.

Table 3. Plasma Cytokines Levels in Six CNPRC SHIV*nef*-Infected Macaques Relative to Four SIV-Infected Monkeys

	Intercepts			*Slope for weeks PI*		
Cytokine	*SIV-infected*	*SHIV*nef-*infected*	p-*Value*	*SIV-infected*	*SHIV*nef-*infected*	p-*Value*
CXCL1	2.90	2.2003	0.0038	0.02	0.0080	0.0825
IFNγ	2.37	1.6011	0.0566	–0.02	0.0074	0.0305
IL-12	0.56	1.6472	0.0002	0.02	0.0038	0.0822
IL-15	2.47	2.2165	0.4359	–0.01	0.0085	0.3986
IL1-Ra	2.57	2.4728	0.5305	000	0.0151	0.0632
IL-8	2.33	2.1582	0.2886	0.01	0.0060	0.6491
G-CSF	0.60	0.7747	0.7988	000	0.0150	0.5153
GM-CSF	–0.16	0.6079	<0.0001	000	0.0033	0.7523
IFN-α	1.70	1.2695	0.3438	–0.01	0.0041	0.6140
IL-18	1.20	1.5184	0.3112	–0.04	–0.0041	0.1065
IL-2	1.39	1.7642	0.4177	0.00	0.0025	0.8589
IP-10	3.42	3.0348	0.1993	0.01	0.0094	0.9240
CCL2	2.42	2.1334	0.0063	0.00	0.0074	0.3074
sCD40 L	2.34	1.1867	0.0002	0.00	0.0108	0.6360

Table shows the linear mixed effects model estimates for group-specific intercepts and slopes for weeks postinfection for each cytokine. SIV, simian immunodeficiency virus.

We found significantly increased levels of the proinflammatory molecules interleukin-12 and GM-CSF in plasma of the SHIV*nef* group. It is known that IL-12 is increased in the serum of patients with scleroderma-associated PAH (30). It is also known that GM-CSF increases inflammatory cell recruitment and exacerbates PAH when the expression of bone morphogenetic receptor type-2 (BMPR-2) is reduced (40). In line with this, bioinformatic predictions based on inflammatory expression in the lungs of our SHIV*nef*-infected macaques and curated databases pointed to inhibition of BMP-2 as a likely involved pathway. BMP-2 is a negative regulator of smooth muscle cell growth associated with familial, idiopathic, and anorexigen-associated PAH (13,22,35). HIV Tat and cocaine also exacerbate BMPR downregulation and increase proliferation of pulmonary vascular smooth muscle cells (11). In addition, the bioinformatics models predicted, with high confidence, activation of the noncanonical NF-κB transcription factor RelB. RelB is a marker of exacerbations in patients with chronic obstructive pulmonary disease (29) and exerts anti-inflammatory effects in smoke-induced pulmonary acute inflammation in mice (49). Tat-transgenic mice exhibit increased RelB in the brain, where RelB may counter-regulate the pathogenic outcomes of HIV Tat (27). Whether the predicted increase in RelB in the lungs of SHIV*nef* macaques reflects the

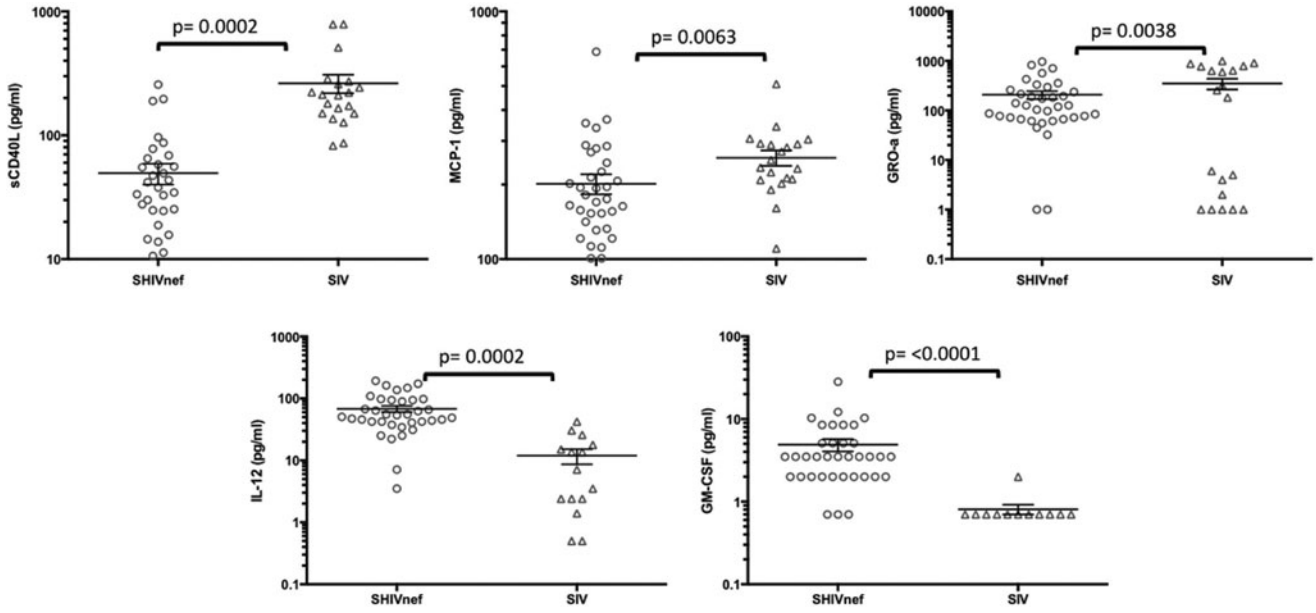

FIG. 12. Detection of inflammatory cytokines in plasma of rhesus macaques infected with SHIV*nef* and SIVmac$_{239}$. Plasma cytokines were measured by Luminex at different times during the course of lentiviral infection. The figure includes the cytokines that were statistically different between the two macaque groups. The *lines* indicate mean with SEM.

TABLE 4. INFLAMMATORY GENE EXPRESSION IN SHIV*NEF* COMPARED TO SIV-INFECTED RHESUS MACAQUES

Gene	*Gene symbol*	*Fold change in SHIV*nef *infection*	*Cellular function/pathway*
Interleukin 12 receptor beta 1 subunit	IL-12RB1	−6.7	JAK-STAT signaling pathway
CD40 ligand	CD40L	−6.4	Immunoglobulin class switch, adaptive immunity
TNF (ligand) superfamily, member 14	TNFSD14	−5.7	NF-kB signaling pathway
Lymphotoxin alpha	LTA	−4.8	Inflammatory, immunostimulatory, and antiviral responses, apoptosis
Chemokine (C-C) ligand 17	CCL17	−4.5	Antimicrobial, trafficking, and activation of mature T cells
Interleukin 3	IL-3	−4.3	Cell growth, differentiation, and apoptosis
Interleukin 1 receptor type 1	IL1R1	−4.1	Interleukin 1 receptor antagonist, MAPK signaling pathway
Fractalkine	CX3CL1	−4.0	T lymphocyte and monocyte chemoattractor
Interleukin 13 receptor subunit alpha-2-like	LOC708339 (Mmu)	−3.4	JAK-STAT signaling pathway
Interleukin 13	IL-13	−3.3	B cell maturation and differentiation
Osteoprotegerin	TNFRSF11B	−3.0	Blocks the binding of TNF-related apoptosis-inducing ligand (TRAIL)
CD70	CD70	−3.0	TNF ligand family, regulates B cell activation
Fas ligand	FasL	−2.8	TNF superfamily, apoptosis
Interleukin 6	IL-6	2.8	Multifunctional cytokine, inflammatory response
Chemokine (C-C) receptor 8	CCR8	2.9	G-protein-coupled receptor signaling pathway
Interferon-inducible T cell alpha chemoattractant	CXCL11	3.0	Chemotactic for activated T cells, CXCR3 signaling pathway
TNF (ligand) superfamily, member 13b	TNFSF13B	3.0	NF-kB signaling pathway
Monocyte chemotactic protein 1	CCL2	3.7	Recruits monocytes, memory T cells, and dendritic cells to the sites of inflammation
Macrophage inflammatory protein 3a	CCL20	3.8	Strongly chemotactic for lymphocytes
Monocyte chemotactic protein 3-like	LOC714751 (Mmu)	4.1	Attracts macrophages during inflammation
Interleukin 1 receptor, type 2	IL-1R2	5.0	MAPK signaling pathway
Macrophage inflammatory protein 3	CCL23	11.6	Highly chemotactic for resting T cells and monocytes

Lung RNA samples were amplified using the PCR targeted array for Rhesus Macaque Inflammatory Cytokines & Receptors (SABiosciences) in a BioRad iCycler iQ, as per manufacturer protocols. The housekeeping genes beta-2-microglobulin and hypoxanthine-guanine phosphoribosyltransferase-like were used for normalization. Gene expression was determined via the $\Delta\Delta C_t$ method; fold changes were calculated based on difference in gene expression between six SHIV*nef*- and two $SIVmac_{239}$-infected macaques. Statistical analyses were not performed given the small sample size in the SIV group. Only the genes with altered expression of genes at fold change cutoff of ±2.7 are shown. Mmu, *Macaca mulatta.*

lung responses to Nef-induced inflammation remains an intriguing question. Taken together, the gene expression results in the lungs of SHIV*nef*-infected macaques are consistent with findings in idiopathic, familial, and HIV-PAH.

We also found significantly lower sCD40 L, CCL2, and CXCL-1 in plasma of SHIV*nef*-infected macaques; sCD40 L was approximately six times decreased in the lungs of SHIV*nef* macaques. Dysregulation of sCD40 L is known to impact immunoglobulin class switching (19) and vascular disease (36). In addition, Nef is known to highjack CD40-dependent immunoglobulin class switching pathways in B cells (37). Hence, our finding of decreased sCD40 L in plasma and lungs of SHIV*nef*-infected macaques compared to SIV-infected monkeys supports potential Nef-mediated immune dysfunction that is evident in the SHIV*nef* model. Surprisingly, we also found significantly decreased CCL-2 in the plasma but ~4X-fold increase in the lungs of SHIV*nef*-infected macaques. CCL-2 is crucial for Th1 immune responses recruitment of macrophages to inflamed tissues (21). Despite the apparent discordance between CCL-2 levels in the periphery and the lung, it is conceivable that CCL-2 redirects the migration of monocytes/macrophages into the lungs in the context of SHIV*nef* infection. Our future studies will measure the levels of the neutrophil recruiter CXCL-1 in the lungs of SHIV*nef*-infected monkeys to relate CXCL-1 levels in the plasma and lungs. Lastly, our finding of increased CCL23 and IL-6 in the lungs of SHIV*nef*-infected monkeys is consistent with PAH associated with systemic sclerosis (48), and idiopathic and familial PAH (23,43), respectively.

Here, we demonstrate the pathobiology of SHIV*nef* infection in rhesus macaques and present compelling evidence that further highlights the Nef-mediated role in PAH-associated pulmonary vascular remodeling using rhesus macaques as models. In addition, we demonstrate that serial passage of chimeric viruses worsens the pulmonary phenotypes and that differences between SIV*nef* and SHIV*nef* may play an important role in the development of severe angioproliferative pulmonary hypertensive disease. Another important contribution of this work is that our findings (summarized in Fig. 14) are concordant with features in

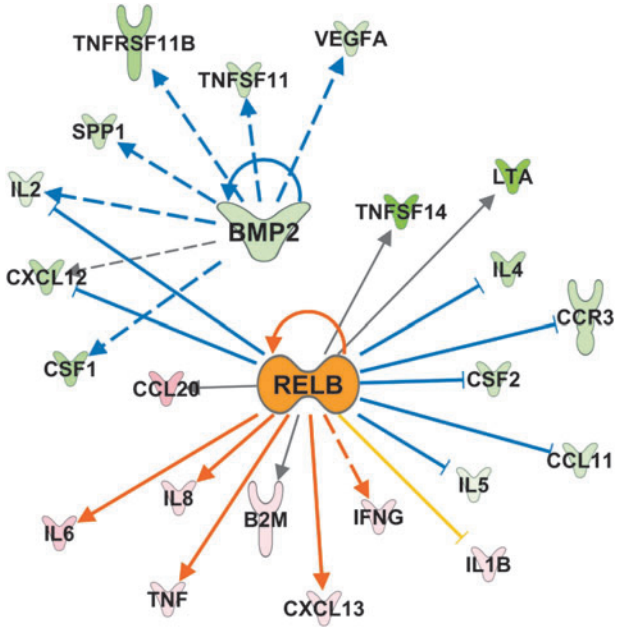

FIG. 13. Inflammatory upstream regulators in the lungs of SHIV*nef*-infected rhesus macaques. Gene expression from 84 inflammatory genes was measured in the lungs of infected rhesus macaques and their direction of change used to identify activated or inhibited upstream regulators affecting the system. BMP-2 (measured directly) and RelB (not measured on the array) were predicted to be the most inhibited (z-score = −2.6) and activated (z-score = 2.8) molecules respectively due to SHIV*nef* infection by the IPA software. Targets known to be induced by BMP-2 are all shown to be down (*green*) in the array, while genes known to either be induced or inhibited by RelB are up (*red/pink*) and down (*green*) respectively. The only downstream target not reflective a more active RelB is IL1B (*yellow line* indicates inconsistent relationship). *Dashed lines* indicate indirect and *solid lines* indicate direct biological relationships between the connected genes, while *blue* (inhibited) and *orange* (activated) *lines* signify the activation state of the effector molecule based on the expression of the connected target.

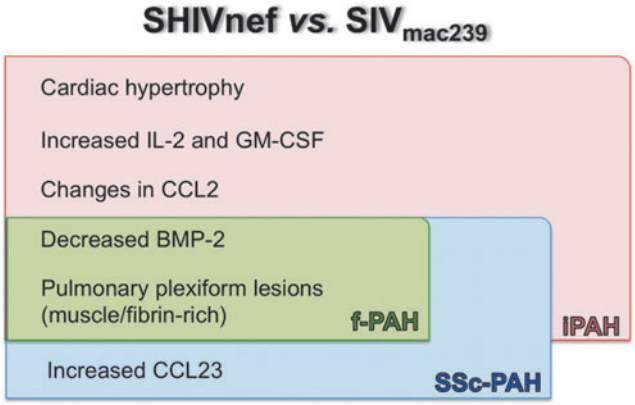

FIG. 14. Summary of differences molecular and histopathological findings between SHIV*nef*- and SIVmac239-infected macaques and concordance with different forms of PAH. The most relevant findings of our study are listed. Most of our observations in SHIV*nef*-infected macaques are consistent with several forms of PAH (iPAH colored in *pink*, Ssc-PAH in *blue*, and f-PAH in *green*). iPAH, idiopathic pulmonary arterial hypertension; fPAH, familial PAH; SSc-PAH, systemic sclerosis-associated PAH.

HIV-PAH, idiopathic PAH, scleroderma PAH, and familial PAH and open the door for future mechanistic studies to elucidate the differences in the nature of PAH-like lesions in the SIV and SHIV*nef* models.

Authors' contributions

Conception and design of the studies (S.C.F., N.F.V., P.A.L.); accountability of all aspects for integrity and accuracy (S.A., S.C.F.); acquisition and analyses of clinical end points (P.A.L., S.V.W.); histology (J.S., J.F., E.C.); inflammatory biomarkers (L.D.G.); parentage and ancestry verification (S.K.); cardiac hypertrophy biomarkers (C.S.L.). Bioinformatic predictions and analyses of lung gene expression data (M.G.E.), statistical analyses (S.A.); article writing (S.A. and S.C.F.); final approval of article (all authors).

Acknowledgments

The authors wish to thank Lourdes Adamson (Center for Comparative Medicine at UC-Davis) for providing expert technical assistance on the virological aspects of the study at CNPRC, Dr. Christopher J. Miller (Department of Pathology, Microbiology & Immunology at UC-Davis) for providing samples from SIV-infected macaques as controls for plasma biomarkers, Dr. Angela Carville (Harvard Medical School) for assistance at NEPRC, and Drs. Andrew D. Miller, Carlyne Cool, and Rubin Tuder for histopathological examinations. Finally, the authors wish to extend a posthumous acknowledgement to Dr. Michael Piatak, Jr for his contribution in measuring SIV viral loads.

This study was supported by the NIH/NHLBI grants R01 HL083491, its supplement under the American Recovery and Reinvestment Act, R01 HL059785 (to SCF), T32-HL007171 (UC-Denver Cardiovascular Physiology Laboratory), and NIH/NCATS UL1 TR001082 (Colorado CTSA), R01 AI096966, and R56 AI080418 (to EC). The CNPRC is supported by the NIH Base Operating Grant OD011107. The NEPRC was supported by NIH/NCRR P51 RR000168, and RR000169. Texas Biomedical Research Institute is supported by OD011133. Content is the authors' sole responsibility and does not necessarily represent official NIH views.

Author Disclosure Statement

No competing financial interests exist.

References

1. Abe K, Toba M, Alzoubi A, *et al.* Formation of plexiform lesions in experimental severe pulmonary arterial hypertension. Circulation 2010;121:2747–2754.
2. Almodovar S, Knight R, Allshouse AA, *et al.* Human Immunodeficiency Virus nef signature sequences are associated with pulmonary hypertension. AIDS Res Hum Retroviruses 2012;28:607–618.
3. Aytekin M, Aulak KS, Haserodt S, *et al.* Abnormal platelet aggregation in idiopathic pulmonary arterial hypertension: role of nitric oxide. Am J Physiol Lung Cell Mol Physiol 2012;302:L512–520.

4. Bjornsson J, and Edwards WD. Primary pulmonary hypertension: a histopathologic study of 80 cases. Mayo Clin Proc 1985;60:16–25.
5. Brown RD, Ambler SK, Li M, *et al.* MAP kinase kinase kinase-2 (MEKK2) regulates hypertrophic remodeling of the right ventricle in hypoxia-induced pulmonary hypertension. Am J Physiol Heart Circ Physiol 2013;304:H269–281.
6. Chalifoux LV, Simon MA, Pauley DR, *et al.* Arteriopathy in macaques infected with simian immunodeficiency virus. Lab Invest 1992;67:338–349.
7. Chen Y, Qin S, Ding Y, *et al.* Reference values of clinical chemistry and hematology parameters in rhesus monkeys (*Macaca mulatta*). Xenotransplantation 2009;16:496–501.
8. Cool CD, Kennedy D, Voelkel NF, *et al.* Pathogenesis and evolution of plexiform lesions in pulmonary hypertension associated with scleroderma and human immunodeficiency virus infection. Hum Pathol 1997;28:434–442.
9. Cota-Gomez A, Flores AC, Ling XF, *et al.* HIV-1 Tat increases oxidant burden in the lungs of transgenic mice. Free Radic Biol Med 2011;51:1697–1707.
10. Courtney CL, Ethun KF, Villinger F, *et al.* Massive occlusive thrombosis of the pulmonary artery in pigtailed macaques chronically infected with R5-tropic simian-human immunodeficiency virus. J Med Primatol 2015;44: 35–39.
11. Dalvi P, O'Brien-Ladner A, and Dhillon NK. Down-regulation of bone morphogenetic protein receptor axis during HIV-1 and cocaine-mediated pulmonary smooth muscle hyperplasia: implications for HIV-related pulmonary arterial hypertension. Arterioscler Thromb Vasc Biol 2013;33:2585–2595.
12. Dalvi P, Wang K, Mermis J, *et al.* HIV-1/cocaine induced oxidative stress disrupts tight junction protein-1 in human pulmonary microvascular endothelial cells: role of Ras/ERK1/2 pathway. PLoS One 2014;9:e85246.
13. Deng Z, Morse JH, Slager SL, *et al.* Familial primary pulmonary hypertension (gene PPH1) is caused by mutations in the bone morphogenetic protein receptor-II gene. Am J Hum Genet 2000;67:737–744.
14. George MP, Brower A, Kling H, *et al.* Pulmonary vascular lesions are common in SIV- and SHIV-env-infected macaques. AIDS Res Hum Retroviruses 2011;27:103–111.
15. George MP, Champion HC, Simon M, *et al.* Physiologic changes in a nonhuman primate model of HIV-associated pulmonary arterial hypertension. Am J Respir Cell Mol Biol 2013;48:374–381.
16. Giavedoni LD. Simultaneous detection of multiple cytokines and chemokines from nonhuman primates using luminex technology. J Immunol Methods 2005;301:89–101.
17. Gill AF, Ahsan MH, Lackner AA, *et al.* Hematologic abnormalities associated with simian immunodeficieny virus (SIV) infection mimic those in HIV infection. J Med Primatol 2012;41:214–224.
18. Green LA, Yi R, Petrusca D, *et al.* HIV envelope protein gp120-induced apoptosis in lung microvascular endothelial cells by concerted upregulation of EMAP II and its receptor, CXCR3. Am J Physiol Lung Cell Mol Physiol 2014; 306:L372–382.
19. Hirbod-Mobarakeh A, Aghamohammadi A, and Rezaei N. Immunoglobulin class switch recombination deficiency type 1 or CD40 ligand deficiency: from bedside to bench and back again. Expert Rev Clin Immunol 2014;10:91–105.
20. Hodara VL, Parodi LM, Chavez D, *et al.* Characterization of gammadeltaT cells in naive and HIV-infected chimpanzees and their responses to T-cell activators *in vitro*. J Med Primatol 2014;43:258–271.
21. Huang DR, Wang J, Kivisakk P, *et al.* Absence of monocyte chemoattractant protein 1 in mice leads to decreased local macrophage recruitment and antigen-specific T helper cell type 1 immune response in experimental autoimmune encephalomyelitis. J Exp Med 2001;193:713–726.
22. Humbert M, Deng Z, Simonneau G, *et al.* BMPR2 germline mutations in pulmonary hypertension associated with fenfluramine derivatives. Eur Respir J 2002;20:518–523.
23. Humbert M, Monti G, Brenot F, *et al.* Increased interleukin-1 and interleukin-6 serum concentrations in severe primary pulmonary hypertension. Am J Respir Crit Care Med 1995;151:1628–1631.
24. Jeong MY, Walker JS, Brown RD, *et al.* AFos inhibits phenylephrine-mediated contractile dysfunction by altering phospholamban phosphorylation. Am J Physiol Heart Circ Physiol 2010;298:H1719–1726.
25. Kanmogne GD, Primeaux C, and Grammas P. Induction of apoptosis and endothelin-1 secretion in primary human lung endothelial cells by HIV-1 gp120 proteins. Biochem Biophys Res Commun 2005;333:1107–1115.
26. Kanthaswamy S, Satkoski J, Kou A, *et al.* Detecting signatures of inter-regional and inter-specific hybridization among the Chinese rhesus macaque specific pathogen-free (SPF) population using single nucleotide polymorphic (SNP) markers. J Med Primatol 2010;39:252–265.
27. Kiebala M, Polesskaya O, Yao Z, *et al.* Nuclear factor-kappa B family member RelB inhibits human immunodeficiency virus-1 Tat-induced tumor necrosis factor-alpha production. PLoS One 2010;5:e11875.
28. Kramer A, Green J, Pollard J, Jr., *et al.* Causal analysis approaches in ingenuity pathway analysis. Bioinformatics 2014;30:523–530.
29. Labonte L, Coulombe P, Zago M, *et al.* Alterations in the expression of the NF-kappaB family member RelB as a novel marker of cardiovascular outcomes during acute exacerbations of chronic obstructive pulmonary disease. PLoS One 2014;9:e112965.
30. Larsen KO, Yndestad A, Sjaastad I, *et al.* Lack of CCR7 induces pulmonary hypertension involving perivascular leukocyte infiltration and inflammation. Am J Physiol Lung Cell Mol Physiol 2011;301:L50–59.
31. Lee JE, Patel K, Almodovar S, *et al.* Dependence of Golgi apparatus integrity on nitric oxide in vascular cells: implications in pulmonary arterial hypertension. Am J Physiol Heart Circ Physiol 2011;300:H1141–H1158.
32. Mandell CP, Reyes RA, Cho K, *et al.* SIV/HIV Nef recombinant virus (SHIVnef) produces simian AIDS in rhesus macaques. Virology 1999;265:235–251.
33. Marecki J, Cool C, Voelkel N, *et al.* Evidence for vascular remodeling in the lungs of macaques infected with simian immunodeficiency virus/HIV NEF recombinant virus. CHEST 2005;128:621S–622S.
34. Marecki JC, Cool CD, Parr JE, *et al.* HIV-1 Nef is associated with complex pulmonary vascular lesions in SHIV-nef-infected macaques. Am J Respir Crit Care Med 2006; 174:437–445.
35. Newman JH, Trembath RC, Morse JA, *et al.* Genetic basis of pulmonary arterial hypertension: current understanding and future directions. J Am Coll Cardiol 2004;43:33S-39S.
36. Pamukcu B, Lip GY, Snezhitskiy V, *et al.* The CD40-CD40 L system in cardiovascular disease. Ann Med 2011; 43:331–340.

37. Qiao X, He B, Chiu A, *et al.* Human immunodeficiency virus 1 Nef suppresses CD40-dependent immunoglobulin class switching in bystander B cells. NatImmunol 2006;7:302–310.
38. Reiser PJ, Portman MA, Ning XH, *et al.* Human cardiac myosin heavy chain isoforms in fetal and failing adult atria and ventricles. Am J Physiol Heart Circ Physiol 2001;280: H1814–1820.
39. Sakao S, Tatsumi K, and Voelkel NF. Endothelial cells and pulmonary arterial hypertension: apoptosis, proliferation, interaction and transdifferentiation. Respir Res 2009;10:95.
40. Sawada H, Saito T, Nickel NP, *et al.* Reduced BMPR2 expression induces GM-CSF translation and macrophage recruitment in humans and mice to exacerbate pulmonary hypertension. J Exp Med 2014;211:263–280.
41. Sehgal PB, Mukhopadhyay S, Patel K, *et al.* Golgi dysfunction is a common feature in idiopathic human pulmonary hypertension and vascular lesions in SHIV-nef-infected macaques. Am J Physiol Lung Cell Mol Physiol 2009;297:L729–L737.
42. Sitbon O, Lascoux-Combe C, Delfraissy JF, *et al.* Prevalence of HIV-related pulmonary arterial hypertension in the current antiretroviral therapy era. Am J Respir Crit Care Med 2008;177:108–113.
43. Soon E, Holmes AM, Treacy CM, *et al.* Elevated levels of inflammatory cytokines predict survival in idiopathic and familial pulmonary arterial hypertension. Circulation 2010; 122:920–927.
44. Spikes L, Dalvi P, Tawfik O, *et al.* Enhanced pulmonary arteriopathy in simian immunodeficiency virus-infected macaques exposed to morphine. Am J Respir Crit Care Med 2012;185:1235–1243.
45. Taylor BJ, and Johnson BD. The pulmonary circulation and exercise responses in the elderly. Semin Respir Crit Care Med 2010;31:528–538.
46. Tuder RM, Groves B, Badesch DB, *et al.* Exuberant endothelial cell growth and elements of inflammation are present in plexiform lesions of pulmonary hypertension. Am J Pathol 1994;144:275–285.
47. Yamamoto K, Burnett JC, Jr., Jougasaki M, *et al.* Superiority of brain natriuretic peptide as a hormonal marker of ventricular systolic and diastolic dysfunction and ventricular hypertrophy. Hypertension 1996;28:988–994.
48. Yanaba K, Yoshizaki A, Muroi E, *et al.* Serum CCL23 levels are increased in patients with systemic sclerosis. Arch Dermatol Res 2011;303:29–34.
49. Zago M, Rico de Souza A, Hecht E, *et al.* The NF-kappaB family member RelB regulates microRNA miR-146a to suppress cigarette smoke-induced COX-2 protein expression in lung fibroblasts. Toxicol Lett 2014;226:107–116.

Address correspondence to:
Dr. Sharilyn Almodovar
Department of Immunology and Molecular Microbiology
Texas Tech University Health Sciences Center
Lubbock, TX 79430

E-mail: sharilyn.almodovar@ttuhsc.edu